THESIS

SYNTHESIS AND DISCOVERY OF MIXED-ANION NITRIDE MATERIALS

Submitted by

Emily N. Storck

Department of Chemistry

In partial fulfillment of the requirements

For the Degree of Master of Science

Colorado State University

Fort Collins, Colorado

Spring 2023

Master's Committee:

Advisor: James R. Neilson

Chris J. Ackerson
Kaka Ma

ABSTRACT

SYNTHESIS AND DISCOVERY OF MIXED-ANION NITRIDE MATERIALS

The ability to synthesize heteroanionic (or mixed-anion) materials is an important area in solid-state chemistry research. Mixed-anion compounds offer the potential to provide more desirable functionality compared to single-anion systems. However, mixed-anion systems are underexplored compared to single-anions. This is especially true for nitride materials when compared to oxides, because nitrides are difficult to make. The ease of making most oxides is due to the reactivity of oxygen and the thermodynamic stability of metal oxides, whereas the strong triple bond of N_2 leads to its low reactivity and therefore difficulty in making nitrides and oxynitrides. Therefore, improved synthetic routes to produce these mixed-anion compounds are needed to unlock the potential of this underexplored phase space. This thesis describes the use of solid-state metathesis reactions to produce heteroanionic ZrNCl through reaction between A_yNCl (A = Zn, Mg, or Li) precursors and $ZrCl_4$. This thesis also highlights the use of flux reactions in attempts to synthesize new oxynitride materials based on the hypothesis that alkali halide salts have the ability to solublize nitrogen and raise its chemical potential relative to the chemical potential of nitrogen in traditional solid-state reactions to produce nitrides and oxynitrides, allowing for incorporation into products to form an oxynitride material. Here, a eutectic flux mix, LiCl-KCl, was used in the reaction between V_2O_3 and Li_3N to synthesize vanadium containing compounds along with preliminary experiments to ascertain their stiochiometry.

ACKNOWLEDGEMENTS

Thank you to my advisor, Jamie Neilson for the help and support throughout the course of this project. I would also like to thank the Analytical Resources Core for use of their instrumentation. I would like to acknowledge the National Science Foundation for funding different aspects of this research. The research presented in Chapter 2 was funded by The National Science Foundation Award DMR-1653863, and the research presented in Chapter 3 was funded by The National Science Foundation Award DMR-2210780.

DEDICATION

For Whiskers, who gave me the moral support I needed.

TABLE OF CONTENTS

LIST OF TABLES

LIST OF FIGURES

Chapter 1

Introduction

1.1 Importance of mixed-anion and oxynitride materials

Throughout the past 100 years of materials research, focus has been on single-anion systems and the different functionality that can result from changes of metal cations. [2] The space of mixed-anion materials is highly underexplored with respect to research on single-anion systems. Both oxide and nitride compounds hold great importance in the field of solid-state chemistry. Both oxides and nitrides are known for their energy and electronic applications such as superconductors, LEDs, energy storage, and photocatalysts. For example, GaN is a material that made such significant contributions to the world of LEDs that Hiroshi Amano, Akasaki Isamu, and Shuji Nakamura won the Nobel prize in 2014 for their work on synthesizing GaN for its use as a blue LED. [3] However, including focus on enhancing properties by introducing multiple anions can allow the field of materials synthesis to grow even further.

Because anions have such specific and unique characteristics (e.g., electronegativity, ionic radii, and polarizability) introducing multiple anions into a structure will inevitably change the properties and characteristics of that structure. For example, replacing one oxygen atom with a different anion in an oxide structure can change the crystal field splitting or the degeneracy in valence orbitals of that structure. [2] This is seen in many perovskites in which many closed-shell oxide perovskites are usually colorless, while their oxynitride analogues show strong visible light absorption. A specific example of this is seen in the solid solution of $CaTaO_2N$ and $LaTaON_2$ which varies in color from yellow to red and could be a good replacement for typical cadmium-based pigments used to produce these colors. [4]

1.2 Challenges for Nitride (and oxynitride) Synthesis

Oxides tend to be easily synthesizable due to the high reactivity of oxygen. Nitrides tend to be much more difficult to synthesize due to a few different factors. To start, nitrides (and oxynitrides) have a lower energy of formation compared to oxides (e.g. formation energies for Zn_3N_2 and ZnO are -0.032 eV/atom and -1.792 eV/atom respectively). However, (oxy)nitrides also have a high cohesive energy and can form strong M-N bonds. This means that once they are formed, they tend to be kinetically stable, meaning metastable phases can become synthetically attainable. [5] However, it also means needing to overcome the energy barrier in M-N bonds of precursors. In order to get past these energy barriers, high temperatures are usually needed. This means that even if present in the system as N^{3-}, nitrogen can easily form into N_2(g) because a high reaction temperature will increase the entropic favorability of forming N_2(g), causing formation of nitrides to be much less likely compared to N_2(g). Because oxides are typically more thermodynamically stable than nitrides (meaning they have a larger enthalpy of formation), it can mean that any oxygen present in a reaction will lead to the formation of metal oxides rather than oxynitrides. However, this thesis highlights some ways in which these synthesis challenges of (oxy)nitrides can be overcome, such as through solid-state metathesis reactions and flux synthesis. These two synthetic techniques were used in order to target two different mixed-anion materials for use in different electronic applications. Solid-state metathesis was used to target ZrNCl, which is a mixed-anion phase that has been seen to be electron doped to become a superconductor. Alkali halide salt flux synthesis was used to target an oxynitride in the Li-V-O-N phase space, with hopes for it to be eventually tested in lithium-ion batteries.

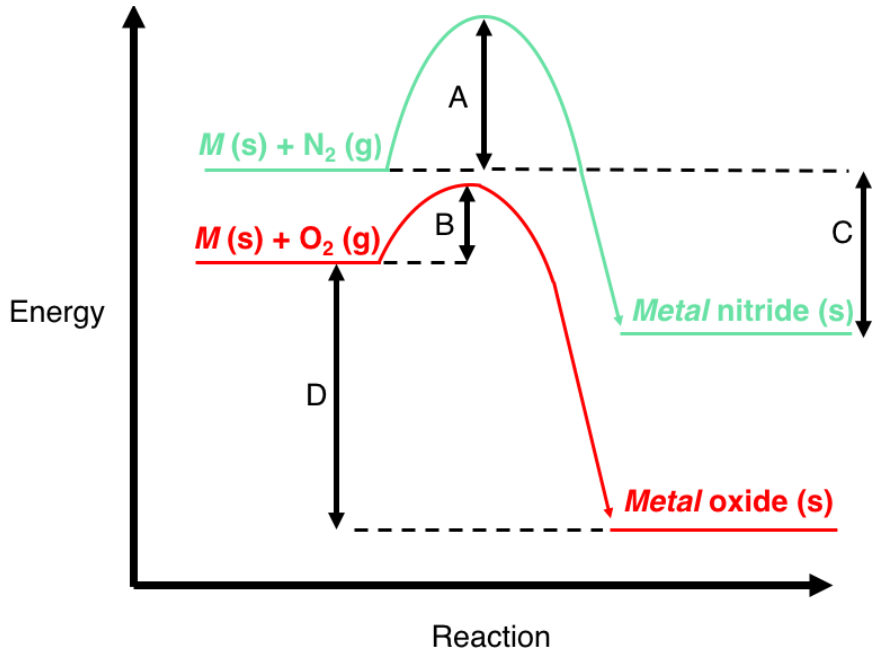

Figure 1.1: Diagram representing the differences in formation and cohesive energy between oxides and nitrides. Oxides have a larger enthalpy of formation than nitrides, which makes them more thermodynamically favorable to form. On the other hand, nitrides have a higher cohesive energy than oxides. It is more energetically taxing to break a M-N bond than a M-O bond.

1.3 Analysis and characterization techniques for mixed-anion and oxynitride materials

1.3.1 Powder X-ray Diffraction

Powder X-ray Diffraction (PXRD) is a technique used for initial characterization of materials to eliminate certain structures as possible products. In PXRD, X-rays are scattered when they interact with the atoms in the powder. The scattering angle is characteristic of the d-spacing between atomic layers in the structure. A peak will show in intensity when the Bragg equation ($n\lambda$=2d $\sin\theta$) is satisfied as constructive interference occurs. In a PXRD experiment, one will survey over a certain 2θ range depending on where it is known that certain reflections may appear. The reason this technique is not all encompassing and cannot be used to fully characterize oxynitrides specifically is that if atoms have a similar electron count (e.g., oxygen and nitrogen), it is not possible to differentiate between the two with X-ray diffraction.

1.3.2 Neutron Diffraction

Neutron diffraction provides complementary information to PXRD about a material. Instead, the diffraction intensity will depend on the atomic isotope rather than the number of electrons. All isotopes have characteristic scattering lengths. Neutron diffraction can therefore be used to determine the presence and difference of oxygen and nitrogen in a structure as they have different scattering lengths (b_c = 5.803 fm for oxygen and b_c = 9.36 fm for nitrogen). [6]

Chapter 2

Synthesis of ZrNCl Through Solid-State Metathesis Reactions

2.1 Introduction

Materials chemists have interests in studying heteroanionic compounds due to their ability to have tunable properties, but they are underexplored compared to single-anion systems. [7] The properties of anions in a material are what often lead to electronic or energetic properties. Therefore, a structure with multiple anions can add more variables which allow for tuning of the structure in order to reach these desired properties. A characteristic example of heteroanionic substitution in oxynitrides is narrowing of the band gap. With substitution of a less electronegative anion, the band gap can narrow due to the valence band being raised in energy. [2] However, controlling anion content is often difficult, particularly with nitrogen. Due to the high cohesive energy present in N_2(g), reactions to make compounds containing nitrogen require high temperatures, making formation of N_2(g) much more entropically favorable than a nitride compound. It can therefore be synthetically difficult to incorporate nitrogen into the desired product in stoichiometric amounts. When trying to synthesize nitrides (or mixed-anion materials containing nitride), it is important to find ways to increase the chemical potential (or reactivity) of nitrogen in the system.

The heteroanionic material, ZrNCl, has attracted interest for its superconducting properties when electron-doped. Figure 2.1 shows a ternary phase diagram of the Zr-N-Cl phase space as well as the crystallographic structure of ZrNCl. Previous reports by Istomin and coworkers highlight the synthesis of ZrNCl through thermal decomposition of $(NH_4)_2ZrCl_6$. [8] A vapor transport technique was used to make the $(NH_4)_2ZrCl_6$ in which the authors combined NH_4Cl and $ZrCl_4$ in a Schlenk tube, thermally treated it at 400 °C for 4 hours, and then placed one end of the tube at 400°C and the other at 100 °C. This causes the $(NH_4)_2ZrCl_6$ to travel to the colder end of

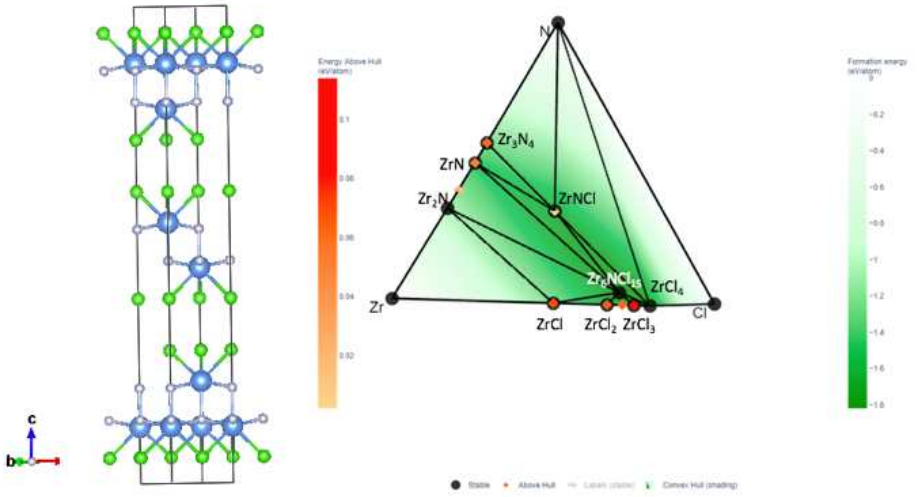

Figure 2.1: $R\bar{3}m$ ZrNCl structure (left), with Zr, N, and Cl atoms being blue, grey, and green respectively. Ternary phase diagram of the Zr-N-Cl phase space (right).

the sealed tube. In a two-zone furnace, $(NH_4)_2ZrCl_6$ was placed in an Ar-filled silica ampoule. The temperature of the furnace where the sample was placed was slowly increased to sublime $(NH_4)_2ZrCl_6$, while the other zone of the furnace was held at a constant, higher temperature. The sublimed material travelled to the hot zone and decomposed into ZrNCl. In another report, synthesis of ZrNCl was completed through the direct reaction of zirconium metal with NH_4Cl at temperatures ranging from 550 °C to 700 °C. Vapor transport was also used in this report in order to purify the ZrNCl of some oxide contamination. [9]

In this work, different synthetic routes to ZrNCl were explored in order to gain a better understanding of how to reach this phase with solid-state metathesis reactions. [10, 11] Metathesis could offer a simple route to ZrNCl with control over anion composition. Metathesis is a double displacement reaction in which ion exchange occurs to form a targeted product plus a salt byproduct. These reactions take the general form $AQ + MX \longrightarrow AX + MQ$, AX being the side product (typically an easy to remove salt) and MQ being the sought after product, which are ACl_z (A = Zn, Mg, or Li) and ZrNCl respectively in this work (balanced equation for this system being A_yNCl + $ZrCl_4 \longrightarrow$ y ACl_z + ZrNCl). [12] Because of this side product and its ability to be separated in

most cases, one can use different precursors to target the same phase, allowing for control over the reaction. For example, previous work has seen that $MgZrN_2$ can be produced from the reaction between $ZrCl_4$ and Mg_2NCl or Mg_3N_2. [13]

2.2 Experimental

2.2.1 Precursor preparation

The precursor, Zn_2NCl was prepared by grinding together equal molar amounts of Zn_3N_2 (99%, Alfa Aesar) (1.0531 ± 0.001g) and $ZnCl_2$ (98%, Sigma Aldrich) (0.6907 g) with a mortar and pestle in an argon filled glove box, sealing these reactants in an evacuated quartz tube, and heating for 20 h at 550 °C, following previous synthesis reports from Liu, et al (balanced reaction is Zn_3N_2 + $ZnCl_2 \longrightarrow 2\ Zn_2NCl$). [14, 15] Mg_2NCl and Li_4NCl were prepared with the same approach, but with equal molar amounts of Mg_3N_2 (99%, Alfa Aesar) (0.5051 ± 0.001g) and $MgCl_2$ (98%, Sigma Aldrich) (0.4653 ± 0.001g) and Li_3N (99%, Alfa Aesar)(0.0707 ± 0.001g) and LiCl (98%, Sigma Aldrich) (0.0864 ± 0.001g), respectively (balanced reactions are Mg_3N_2 + $MgCl_2 \longrightarrow 2$ Mg_2NCl and Li_3N + LiCl $\longrightarrow$ Li_4NCl). [16, 17]

2.2.2 Solid-state metathesis reactions to make ZrNCl

Reagents (A_yNCl and $ZrCl_4$ (98%, Acros Organics)) were combined by grinding powders with a mortar and pestle air-free in an argon-filled glove box with oxygen and water levels monitored to be below 1 ppm. Reaction between Zn_2NCl + $ZrCl_4$, Mg_2NCl + $ZrCl_4$, and Li_4NCl + $ZrCl_4$ were all completed with molar ratios of 0.4:1, 0.6:1, 0.8:1, and 1:1 of the A_yNCl to $ZrCl_4$ respectively to successfully make ZrNCl. In a glovebox, the mixtures were added to quartz tubes (10 mm inner diameter, 12 mm outer diameter) and capped with parafilm. Parafilm capped tubes were removed from the glove box and immediately sealed under vacuum (p <25 mTorr) using a methane/oxygen torch. Samples were heated in muffle furnaces with 10 °C/min heating rates, 12 h dwell times, variable dwell temperatures, and furnace cooled.

2.2.3 Powder X-ray diffraction

Powder X-ray diffraction (PXRD) patterns were collected on a Bruker D8 Discover DaVinci Powder X-ray Diffractometer with a Cu Kα radiation and a Lynxeye XE-T position-sensitive detector, using 2θ ranges of 5-60° or 10-60°. The powder samples were mounted on a zero diffraction Si wafer with amorphous hydrocarbon grease. All samples were prepared air-free in an argon glove box and covered with polyimide tape during data collection. Diffraction patterns were analyzed and modeled using the Rietveld method in TOPAS6. Data were analyzed using known structures that have been reported in the Inorganic Crystal Structure Database (ICSD) or in the Materials Project.

2.3 Optimization of Metathesis Reactions to make ZrNCl

Initially, attempts to synthesize ZrNCl were completed through reaction between Zn_2NCl + $ZrCl_4$ with Zn_2NCl in excess. It was assumed that metathesis reactions within this phase space would produce the targeted material due to the successful synthesis of $MgZrN_2$ by similar techniques. [13] In that work, it was seen that $MgZrN_2$ was produced at a reaction temperature of 800 °C. Using that as a guide, a reaction was run at 800 °C and held for 12 h. Figure 2.2 shows the results of this reaction (reaction was 2 Zn_2NCl + $ZrCl_4$). Instead of the desired ZrNCl ternary, ZrN was produced.

As seen in Figure 2.2, ZrN was the main product from this reaction. [18] Peaks that do not match with the refinement are excess precursors and the salt byproduct, $ZnCl_2$. The PXRD data was analyzed with the Rietveld method in which a structure of ZrN reported in the ICSD was used in the analysis. Since the refinement in orange fits the data in black, it can be concluded that the main structure present is ZrN. It is not unusual that the reaction reached the ZrN phase rather than ZrNCl. In similar work, for which the target product was $MgZrN_2$, it was shown that the formation of ZrN is the most exothermic formation per atom at a synthesis temperature of 1000 °C. [13] In the ceramic synthesis between Mg_3N_2, Zr, and N_2 to reach $MgZrN_2$, ZrN is the first phase to form. [13] A subsequent reaction occurs to yield $MgZrN_2$ and while this reaction is

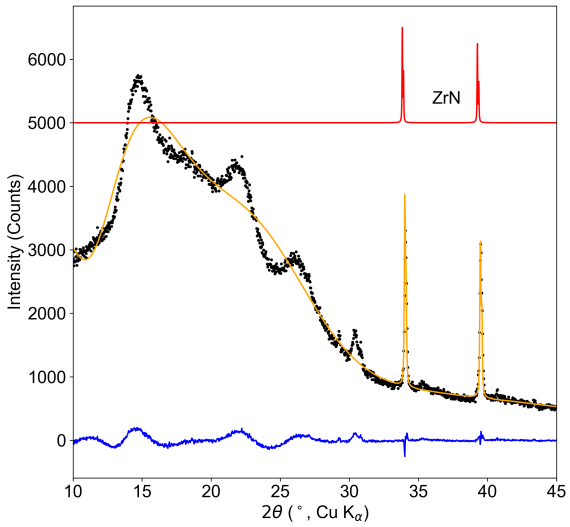

Figure 2.2: Powder X-ray diffraction data of the products from the reaction, 2 Zn_2NCl+$ZrCl_4$, illustrating the primary presence of ZrN. Data shown in black circles, and the calculated pattern (determined from the Rietveld method) is shown in orange. The large background at low angles is a result from the polyimide tape. Peaks around 50° 2θ were unable to be matched with any experimentally made phases in the Zn-Zr-N-Cl phase space. The curve in blue is the difference plot between the refinement and the data.

exothermic, ZrN acts a diffusion barrier to prevent atom migration. [19] Once this phase is made, further reactions are less favorable due to production of the ZrN diffusion barrier.

By using an implementation of the computational framework developed in [20] found in the Materials Project interface reactions predictor, we verified that the reaction between Zn_2NCl and $ZrCl_4$ should produce ZrNCl and $ZnCl_2$ (with a balanced reaction of $Zn_2NCl + ZrCl_4 \longrightarrow ZrNCl + 2\ ZnCl_2$). So, reactions between Zn_2NCl and $ZrCl_4$ were completed with ratios varying from 0.4:1 to 1:1 respectively at 800 °C and held at this temperature for 12 h. Figure 2.3 shows the results of these reactions. Production of ZrNCl occured at each ratio along with the salt byproduct, $ZnCl_2$. However, excess precursors remained in the reaction. Also, at the highest ratio of 1:1, ZrN was produced.

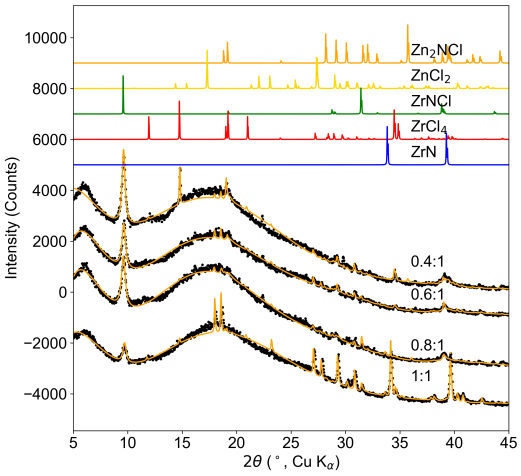

Figure 2.3: Powder X-ray diffraction data of the products from reactions between Zn_2NCl and $ZrCl_4$, illustrating the presence of predicted products ZrNCl and $ZnCl_2$ along with unreacted precursors. Ratios are of Zn_2NCl:$ZrCl_4$ respectively. Data shown in black circles, and the calculated pattern (determined from the Rietveld method) is shown in orange. The large background at low angles is a result from the polyimide tape. Calculated patterns of precursors and hypothesized products are shown in the top of the plot.

Again, by applying the same implementation of [20] found in the Materials Project interface reactions predictor, reaction between Mg_2NCl and $ZrCl_4$ should produce ZrNCl and $MgCl_2$ (with a balanced reaction of $Mg_2NCl + ZrCl_4 \longrightarrow ZrNCl + 2\ MgCl_2$). So, reactions between Mg_2NCl and $ZrCl_4$ were completed with ratios varying from 0.4:1 to 1:1 respectively at 800 °C and held at this temperature for 12 h. Figure 2.4 shows the results of these reactions. Again, as in the Zn system, ZrNCl was produced at each ratio along with the salt byproduct, $MgCl_2$. Excess precursors were still in the system and ZrN was produced at the 1:1 ratio.

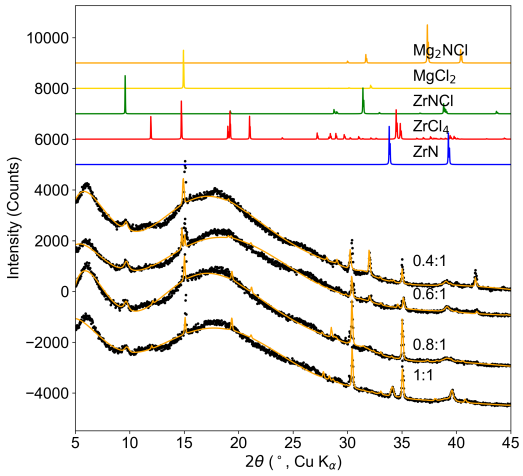

Figure 2.4: Powder X-ray diffraction data of the products from reactions between Mg_2NCl and $ZrCl_4$, illustrating the presence of predicted products ZrNCl and $MgCl_2$ along with unreacted precursors. Ratios are of Mg_2NCl:$ZrCl_4$ respectively. Data shown in black circles, and the calculated pattern (determined from the Rietveld method) is shown in orange. The large background at low angles is a result from the polyimide tape. Calculated patterns of precursors and hypothesized products are shown in the top of the plot.

Lastly, from the Materials Project interface reactions predictor, reaction between Li_4NCl and $ZrCl_4$ should produce ZrNCl and LiCl (with a balanced reaction of $Li_4NCl + ZrCl_4 \longrightarrow ZrNCl + 4\ LiCl$). Again, because of this, reactions between Li_4NCl and $ZrCl_4$ were carried out also with ratios varying from 0.4:1 to 1:1 respectively at 800 °C and held at this temperature for 12 h. Results of these reactions are seen in Figure 2.5 and can be described in a somewhat similar fashion to both the zinc and magnesium systems. Products of ZrNCl and LiCl were seen and excess precursors were present in each reaction. At the 1:1 ratio, formation of ZrN can be seen.

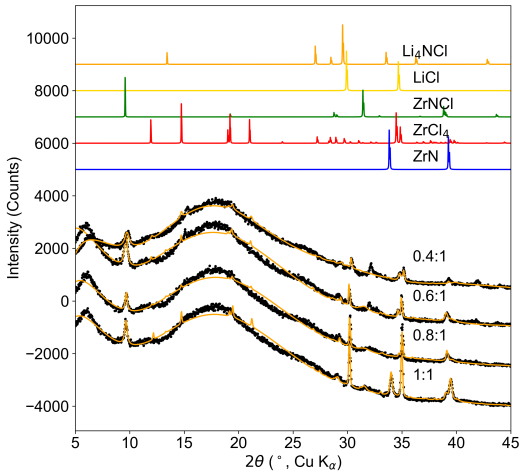

Figure 2.5: Powder X-ray diffraction data of the products from reactions between Li_4NCl and $ZrCl_4$, illustrating the presence of predicted products ZrNCl and LiCl along with unreacted precursors. Ratios are of Li_4NCl:$ZrCl_4$ respectively. Data shown in black circles, and the calculated pattern (determined from the Rietveld method) is shown in orange. The large background at low angles is a result from the polyimide tape. Calculated patterns of precursors and hypothesized products are shown in the top of the plot.

As can be seen in Figures 2.3 - 2.5, reactivity occurred in each system and ZrNCl was made in each reaction. However, because excess precursors were present, it was thought that the anneal temperature of the reactions could be too low, meaning that the reactions had not fully equilibrated. However, because excuess $ZrCl_4$ is included in the reaction, it would makes sense that there would be some leftover at the end of the reaction based on stoichiometry. It was also seen that lower ratios of A_yNCl to $ZrCl_4$ avoided the production of ZrN. Because of these two factors, subsequent reactions were performed with a ratio of 0.4:1 of A_yNCl to $ZrCl_4$ respectively and were reacted at a temperature of 980 °C. Figure 2.6 is the PXRD plots from these reactions. A future direction that could be taken would be to attempt reactions at 980 °C with varying ratios of A_yNCl to $ZrCl_4$. Quantification of ZrNCl production at both 800 °C and 980 °C and their varying ratios could be completed to determine the optimum temperature and ratio for making ZrNCl.

2.4 Conclusion

A mixed-anion phase, ZrNCl, was made through solid-state metathesis. It was found that lower ratios of A_yNCl (A= Zn, Mg, or Li) to $ZrCl_4$ were best for making this product and avoiding production of ZrN. The ratio of 0.4:1 was concluded to be the best ratio. When too much N is included in the reaction, the ZrN phase is reached and further reactio cannot be completed to reach the desired product, ZrNCl, as ZrN acts as a diffusion barrier. On the other hand, if too much $ZrCl_4$ is included in the reaction, it will be leftover in the product as excess precursor due to stoichiometry. Unlike, ZrN, $ZrCl_4$ can be removed and separated from the desired prodcut.

2.5 Outlook and Future Work

As can be seen in Figure 2.6, annealing at 980 °C allowed for ZrNCl production. However, both $ZrCl_4$ and the salt byproducts were also present. A route to be taken is to purify the ZrNCl of excess $ZrCl_4$ and any salt byproduct. A few different methods can be attempted to try to achieve this. The first would be to complete a solvent wash of the product, which could potentially allow for the excess $ZrCl_4$ and salt to be washed away from the desired ZrNCl product. [21] Both $ZrCl_4$ and the salts are soluble in methanol, hexanol, and water. Separate wash and dry processes with all of these solvents would be completed and X-ray analysis should be done to measure success and determine which solvent would be best for achieving purified ZrNCl. An issue that could arise with solvent washing is intercalation of ZrNCl which has been shown to occur. [22] Another option to purify the ZrNCl and get rid of the salts would be to use vapor transport. [23, 24] In a tube furnace, a sealed tube will be placed with the sample at a hot enough temperature to evaporate the salt, but not hot enough to transport the ZrNCl. The cold end of the furnace should be set below the melting points of each respective salt. Over time, the salt will transport and deposit at the cold end, leaving ZrNCl at the hot end of the tube.

Varying the ratio of precursors at the higher temperature (980 °C) should be attempted so that the same ratios for both temperatures are done and the quantification of ZrNCl can be completed to determine the best ratio and temperature for making ZrNCl through metathesis reactions. Improv-

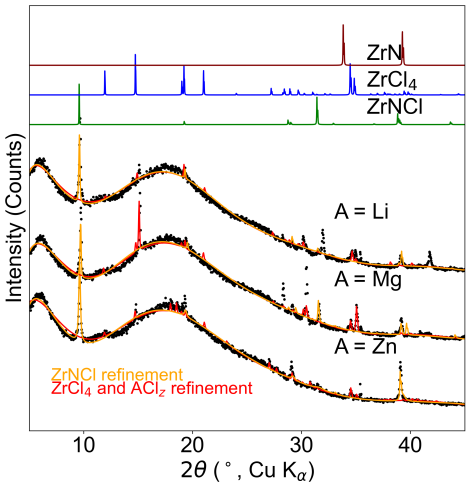

Figure 2.6: Powder X-ray diffraction data of the products from reactions between A_yNCl and $ZrCl_4$ at a 0.4:1 ratio respectively. This plot shows the presence of predicted products ZrNCl and ACl_z along with excess $ZrCl_4$. Data shown in black circles, and the calculated patterns (determined from the Rietveld method) are shown in orange (ZrNCl) and red ($ZrCl_4$ and ACl_z). The large background at low agnles is a result from the polymide tape.

ing the purity of the final product is also important. There are multiple ways that could possibly allow for this, including solvent washing and vapor transport purification. Once purification is achieved, attempt at determining if ZrNCl has been doped by precursor cations (Zn, Mg, and Li) should be completed as ZrNCl is a superconductor with the ability to be electron doped. Doping the structure with different cations would likely lead to different properties which could be studied.

A main reason for focus on ZrNCl is its ability to be electron doped to become a superconductor. A question that has yet to be answered is if any cation intercalation has already happened in the metathesis syntheses. On its own, ZrNCl is a band insulator, but when intercalation of Li (or other alkali-metals) atoms occurs, it becomes a superconductor with a T_c of 13 K. Figure 2.7 shows the structure of Li doped ZrNCl. Li intercalates into the Van der Waals gaps between chlorine atoms. [25] The ZrNCl structure can be intercalated very readily as seen in the many reports of this occurrence. For example, Fogg and coworkers share its ability to be intercalated with multiple different metallocenes. [22] One way to measure this would be to prepare phase-pure ZrNCl through the vapor transport technique reported by Istomin. [8] PXRD data of solid-state metathesis

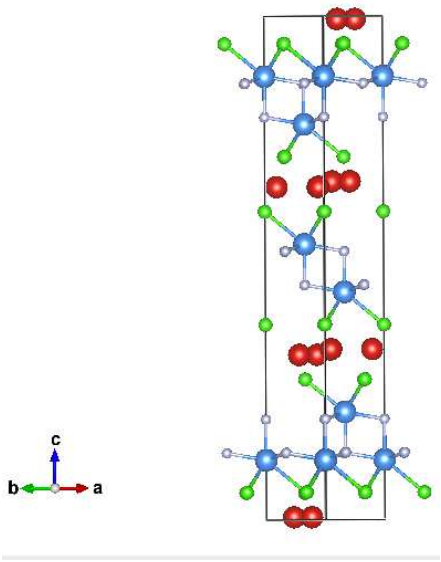

Figure 2.7: Structure of Li_xZrNCl with Li, Zr, N, and Cl being red, blue, grey and green respectively. As discussed above, Li is inserted into the Van der Waals gaps between chlorine atoms in the ZrNCl structure. [1]

prepared ZrNCl could then be compared to this phase-pure substance. If metal intercalation has occurred, a shift towards a lower 2θ would be seen as the unit cell volume would increase, which, according to Bragg's Law, causes this lower 2θ shift. Another way to see intercalation would be to measure superconductive properties. If intercalation of the cations into the Van der Waals gaps between chlorine atoms has already occurred, this could be another benefit to these solid-state metathesis reactions. Instead of using another method and a second step to incorporate the cations into the structure, this could be done in a one-step metathesis reaction.

Chapter 3

Synthesis of Lithium Vanadium Oxynitrides

3.1 Introduction

Materials containing mixed-anions can result in enhanced and unique properties that are not present in their single-anion analogues. However, the stability of nitrogen makes it difficult to incorporate into final products as it can leave the material as N_2(g) during synthesis. This work focused on using a hypothesis that nitride anions are soluble and reactive in halide salts in order to make new oxynitride materials. Currently, the most common synthesis technique to make oxynitrides is ammonolysis which involves reacting oxides with ammonia gas at high temperatures (600-1000 °C). [26, 27] The issue with this approach is that at temperatures above 400 °C, NH_3(g) is highly reducing and will decompose into N_2 and $3H_2$. The reducing conditions will also produce reduced metals, specifically when targeting compounds with d-electron containing metals as they are especially prone to reduction. In addition, it is difficult to control anion composition with ammonolysis, given that the final nitrogen content is dependent on the synthesis temperature and the flow rate of NH_3(g). Finding routes to make oxynitrides at lower temperatures is important in order to keep the chemical potential of nitrogen high and allow for stoichiometric incorporation in the final product. [28]

An approach that can help control the reactivity of nitrogen in reactions is needed and will allow for the ability to target a wider range of oxynitride materials. Our hypothesis is that alkali halide salts can solubilize nitrogen and lead to the selective synthesis of oxynitrides by preventing the release of N_2(g) in intermediate steps. The salt can be present in the reaction after formation through metathesis (e.g., $Li_4NCl + MOCl \longrightarrow 2LiCl + Li_2MON$) or as a flux (e.g., $Li_3N + V_2O_3$ + LiCl). The use of a salt flux can pin the chemical potential of nitrogen at a value high enough to reach the AMNO (oxynitride) phase [29]. If the chemical potential value of nitrogen is too low, reaction between AN (an alkali nitride) and MO (a metal oxide) will proceed towards AO + M

+ N_2(g). The release of nitrogen as N_2(g) tends to be kinetically favored and irreversible because of the significant entropy production that occurs. This blocks the re-formation of a nitride species as nitrogen is no longer chemically available to participate in the reaction. [13, 30] However, the goal is for the salt flux to pin the nitrogen chemical potential given that the interface of AN and MO is in contact with the molten flux. [29, 31, 32] The alkalki nitride, Li_3N, is partially soluble in LiCl with an activity coefficient of 0.25 and chemical potential of nitrogen of -0.75 eV/atom at 900K. [33, 34] This may not be sufficient, however, to reach the oxynitride phase with compounds that have transition metals containing d-electrons as these tend to be reluctant nitride former. This means that the reaction will still proceed towards the formation of N_2(g). In eutectic LiCl-KCl solution, the activity coefficient of nitrogen approaches 1 between 723-900K, giving a chemical potential of -0.25 eV/atom. [35] Because the chemical potential of N_2 is pinned higher in this eutectic flux and the activity coefficient approaches 1, this could potentially allow the formation of AMNO avoiding the irreversible formation of N_2(g).

3.2 Experimental

3.2.1 Precursor preparation

The precursor, V_2O_3 was prepared by grinding V_2O_5 ($\sim$3g) (Sigma-Aldrich) with an agate mortar and pestle and placing in an alumina boat. The boat was placed in a quartz tube in a tube furnace with metal endcaps connected to a flow of 5% H_2/Ar at 1 atm. This gas was flown over the reaction to allow for the reduction from V^{5+} to V^{3+} and heated at 750 °C for 20 h. This heating schedule with flow of H_2/Ar(g) is repeated two more times to allow for full reduction to V_2O_3. [36] VO_2 was prepared by combining V_2O_3 (0.7499g) and V_2O_5 (0.9096g) by grinding them together in a mortar and pestle in an argon filled glovebox, pressing into a pellet, sealing in an evacuated (25 mTorr) quartz tube, and heating at 900 °C for 16 h. [37] A eutectic LiCl-KCl solution was made by combining anhydrous LiCl (1.0600 g, 98%, Sigma Aldrich) and KCl (2.8000 g, 98%, Sigma Aldrich) at a ratio of 0.4: 0.6 moles by grinding until uniform in an agate mortar and pestle in an argon filled glovebox.

3.2.2 Flux reactions to make Li-V-O-N compounds

Reagents (V_2O_3 and Li_3N) were combined by grinding powders with a mortar and pestle in an argon filled glove box. Reactions were completed with molar ratios of 4:1, 2:1, 1:1, 1:2, 1:3, and 1:4 of V_2O_3 (0.1049g-0.2098g) to Li_3N (0.0112g-0.0744g, 99%, Alfa Aesar) respectively. All reactions used a 10 mole ratio of flux (either LiCl (0.4282g) or LiCl-KCl (0.3915g)) which was added directly to either 4.5x7.5mm or 6.5x9.5mm stainless steel tubes. The reagent mix was added to the steel tube on top of the flux. Steel tubes were crimped in the glove box and capped with parafilm. Parafilm capped tubes were removed from the glove box and sealed with an arc welder after being evacuated to be air-free. Once sealed, steel tubes were placed in quartz tubes and quartz were sealed under vacuum (25 mTorr). Samples were heated in muffle furnaces with 5 °C/min heating rates, variable dwell times, variable dwell temperatures, and furnace cooled. Reactions were washed of excess salt flux with methanol in air.

Reactions with the reagents V_2O_3, VO_2, and Li_3N were also completed by grinding all three reagents in a mortar and pestle in an argon filled glovebox. These reactions were completed with molar ratios of 1:2:1 (0.2152g, 0.2356, 0.0483g) and 0.5:1:2 (0.1076g, 0.1178g, 0.0965g) of V_2O_3 to VO_2 to Li_3N respectively and also with a 10 mole ratio of LiCl-KCl flux (0.3915g), which was added directly to stainless steel tubes. The regent mix was then added to the steel tube on top of the flux. Tubes were crimped in the glovebox, capped with parafilm, removed from the glovebox, and sealed with an arc welder after being evacuated. Steel tubes were then placed in quartz tubes and quartz tubes were sealed under vacuum (25 mTorr). Samples were heated in muffled furnaces with 5 °C/min heating rates and held at 500 °C for 12 h. Reactions were washed of excess salt flux with methanol in air.

3.2.3 Powder X-ray diffraction

Powder X-ray diffraction (PXRD) patterns were collected on a Bruker D8 Discover DaVinci Powder X-ray Diffractometer with a Cu Kα radiation and a Lynxeye XE-T position-sensitive detector, using 2θ ranges of 10-100°. The powder samples were mounted on a zero diffraction Si

wafer with amorphous hydrocarbon grease. Samples were prepared in air. Diffraction patterns were analyzed with the Rietveld method in TOPAS5. Data were analyzied using known structures that have been reported in the Inorganic Crystal Structure Database (ICSD) or in the Materials Project.

3.3 Analysis of Results of Flux Reactions

Initially, the first flux reaction was completed with the salt flux LiCl rather than the LiCl-KCl eutectic. Ratio between V_2O_3 and Li_3N was 1:2 respectively and reaction was held at 500 °C for 48 h. As expected based on the previously stated hypothesis, an oxynitride was not formed. Instead, a V-N phase (V_2N) and VO were produced as can be seen in Figure 3.1. This suggests that the chemical potential of nitrogen is too low to produce an oxyntitride. If chemical potential is too low even with an infinite amount of nitrogen available, the nitrogen can leave the solid compound, thus forming N2(g) and causing reduction of the metal. Since the reduced vanadium compound, V_2N, was produced, this suggests the system was under reducing conditions. Because the product of VO was also obsereved, this further inidcates that the chemical potential of nitrogen was too low.

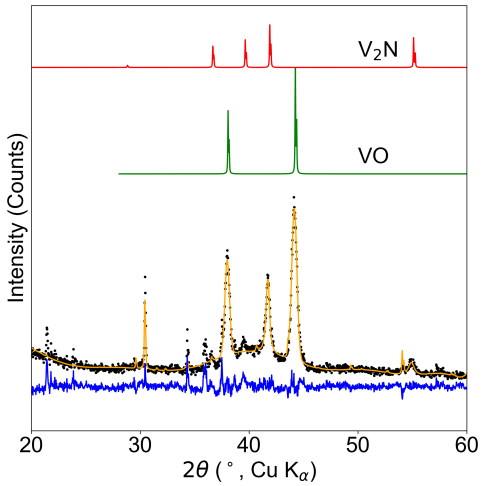

Figure 3.1: Powder X-ray diffraction data of the products from reaction between V_2O_3 and Li_3N in a LiCl flux, illustrating the presence of products V_2N and VO. Data shown in black circles, and the calculated pattern (determined from the Rietveld method) is shown in orange. Calculated patterns of precursors and hypothesized products are shown in the top of the plot. The curve in blue is the difference plot between the refinement and the data.

To test the hypothesis that a LiCl-KCl flux will increase the chemical potential of nitrogen high enough to reach an oxynitride phase, a reaction was completed with the eutectic mix. This reaction was done with a 1:2 ratio of V_2O_3 to Li_3N respectively and held at 500 °C for 48 h. The PXRD data from this reaction can be indexed to the phases: Li_3VO_4 and $LiVO_2$ shown in Figure 3.2.

Table 3.1: Summary of results from reactions of varying ratios between V_2O_3 and Li_3N. The listed phases are known oxides or nitrides that each reaction's PXRD data was indexed to.

V_2O_3:Li_3N	Indexed Known Oxides or Nitrides
4:1	Li_3VO_4 + $LiVO_2$
2:1	$LiVO_2$
1:1	$LiVO_2$
1:2	Li_3VO_4 + $LiVO_2$
1:3	V_8N
1:4	V_8N

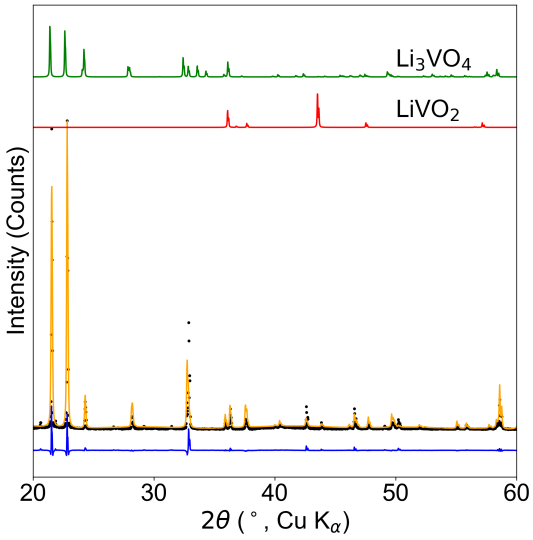

Figure 3.2: Powder X-ray diffraction data of the products from reaction between V_2O_3 and Li_3N in a LiCl-KCl eutectic flux, Data was indexed to the known oxides, Li_3VO_4 and $LiVO_2$. Data shown in black circles, and the calculated pattern (determined from the Rietveld method) is shown in orange. Calculated patterns of precursors and hypothesized products are shown in the top of the plot. The curve in blue is the difference plot between the refinement and the data.

More reactions with varying ratios between V_2O_3, Li_3N and the LiCl-KCl flux were completed at a dwell temperature of 500 °C and a dwell time of 12 h. Results from these reactions are outlined in Table 3.1. The compounds listed in the products column are those that were indexed and refined to the PXRD data collected after each reaction. However, it can be inferred that these exact phases are not what are actually present as the lattice parameters are distinct from that of these oxides.

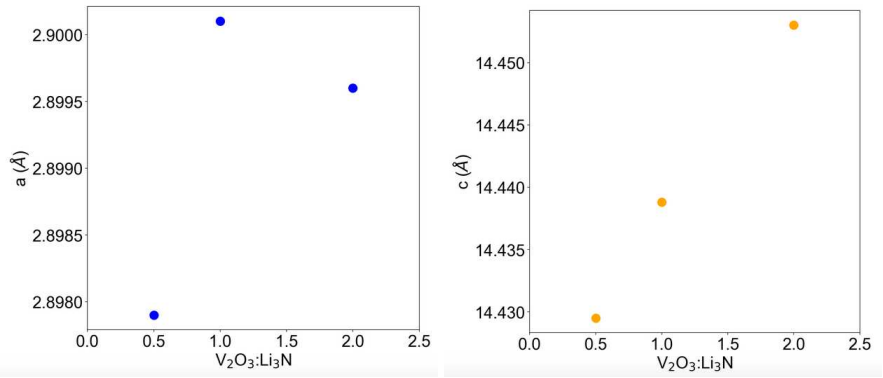

Figure 3.3: The left figure is a plot of ratio of V_2O_3 to Li_3N vs lattice parameter a to show that the a lattice parameter decreases with increasing fraction of V_2O_3. The right figure is a plot of ratio of V_2O_3 to Li_3N vs lattice parameter c to show that the c lattice parameter increases with increasing fraction of V_2O_3.

Most reactions could be indexed to either Li_3VO_4, $LiVO_2$ or both, but as mentioned previously the lattice parameters of the product phases are distinct to those of the oxides. However, with Li_3N content at a ratio of V_2O_3 to Li_3N of 1:3 or more, V_8N is formed. It was concluded that when enough Li_3N is included in the reaction, it puts the system under highly reducing conditions which leads to this reduced vanadium compound. For each of the different ratio reactions (not including the reactions that formed V_8N), the PXRD data was analyzed with the Rietveld method using a known structure of $LiVO_2$. The a and c lattice parameters for each determined from this method were then plotted against the ratio between V_2O_3 and Li_3N used for the reaction as seen in Figure 3.3.

The trend in the change of lattice parameters suggests that nitrogen is possibly being incorporated into the final product. Deintercalation of lithium from Li_xVO_2 can occur and causes a change in lattice parameter values. However, in Li_xVO_2 deintercalation causes the a axis to expand and the c axis to shrink, also causing the oxidation of vanadium. [38] As we increase the fraction of V_2O_3 included in the reaction, the product has lattice parameters closer to those reported for $LiVO_2$, suggesting that the composition is closer to that of $LiVO_2$ than any putative new oxynitrides. As we increase the fraction of Li_3N included in the reaction, we observe the a axis shrink and the c axis expand. Because this is the opposite trend seen when lithium is deintercalated from the Li_xVO_2 structure, we assume that lithium is being stuffed into the unit cell in order to charge compensate

for the inclusion of nitrogen and the oxidation state of vanadium is being held constant because the color of the final product is black, indicating vanadium in the 3+ oxidation state. If we assume that vanadium is not oxidized or reduced from the V^{3+} starting material, this suggests that the composition of the material with excess lithium is described by: $Li_{1+x}V^{3+}O_{2-x}N_x$.

Oxidation titration reactions were also completed in which VO_2 was included as a precursor in the reaction as the vanadium is at a different oxidation state than in V_2O_3. These reactions were also completed at 500 °C and held at this temperature for 12 h. Table 3.2 outlines the results of these titration reactions. Similar to the previous set of reactions, the PXRD data was analyzed with the Rietveld method using the reported crystal structure of $LiVO_2$. The a and c lattice parameters for each were plotted against the amount of VO_2 relative to V_2O_3. For the samples containing a relatively low amount of nitrogen, the lattice parameters are close to that of $LiVO_2$. However, when V^{4+} is added intentionally with a relatively high amount of nitrogen, the lattice parameters venture away from those of $LiVO_2$. As V^{4+} is included in the reaction, it would be expected that the a axis would expand due to intralayer repulsion to avoid V^{4+}-V^{4+} interactions and that the c axis would shrink because of interlayer attraction for improved electrostatics. As can be seen in Figure 3.4, this is what is observed and leads to the conclusion that nitrogen is being incorporated into the final product to charge compensate for the vanadium at a higher oxidation state. It is believed that the following defect is what occurs when V^{4+} is included in the reaction: $LiV^{3+}{}_{1-x}V^{4+}{}_xO_{2-x}N_x$. In the future, data points included between the current two data points is needed in order to have a full picture of what is occurring in these oxidation titration reactions.

Table 3.2: Summary of results from reactions of varying ratios between V_2O_3, Li_3N, and VO_2. The listed phases are known oxides or nitrides that each reaction's PXRD data was indexed to.

V_2O_3:Li_3N:VO_2	Indexed Known Oxides
1:1:2	$LiVO_2$
0.5:2:1	$LiVO_2$

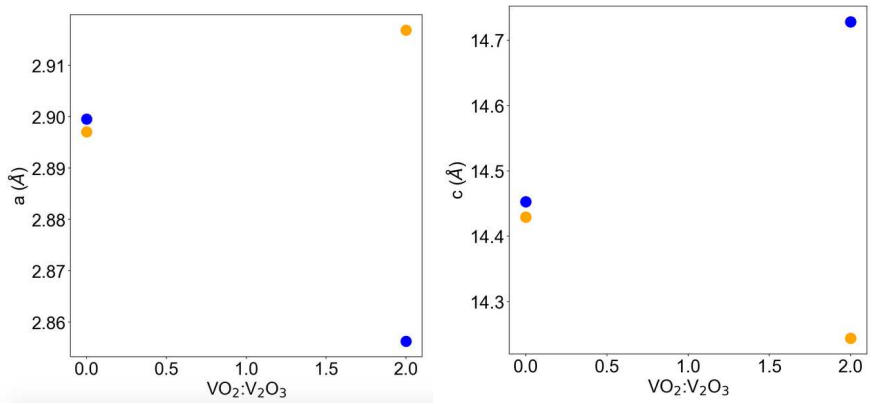

Figure 3.4: The left figure is a plot of ratio of VO_2 to V_2O_3 vs lattice parameter a to show that the lattice parameter increases with increasing fraction of VO_2 at sufficient nitrogen content (orange). The right figure is a plot of ratio of VO_2 to V_2O_3 vs lattice parameter c to show that the lattice parameter decreases with increasing fraction of VO_2 at sufficient nitrogen content(orange). Blue dots represent the lattice parameter change for a ratio of 1:4 nitrogen to vanadium. Orange dots represent the lattice parameter change for a ratio of 1:1 nitrogen to vanadium.

3.4 Conclusion

It has been shown that the hypothesis that the LiCl-KCl alkali salt flux can solubilize nitrogen and lead to the synthesis of oxynitrides by preventing the release of nitrogen due to the increase in chemical potential is likely true by analyzing the change in lattice parameters of the indexed structure in varying ratio reactions. It was also shown that the LiCl flux likely does not raise the chemical potential of nitrogen high enough to produce an oxynitride as seen by the production of V_2 and VO. For the varying ratio reactions, the lattice parameters changed in such a way that indicated the incorporation of nitrogen into the structure for both keeping the oxidation state of vanadium constant and also purposefully introducing vanadium at a different oxidation state. For titration reactions in which the ratio between V_2O_3 and Li_3N was varied, the a and c lattice parameter changes followed the opposite trend of what is seen in the deintercalation of lithium in Li_xVO_2. This inidcates the incorporation of lithium into the structure along with nitrogen to allow for chare compensation. In titration reactions in which the oxidation state of vanadium was varied, when sufficient nitrogen content is provided in the reaction, the a lattice parameter expands and the c lattice parameter shrinks. This indicates the inclusion of V^{4+} in the structure and it can be assumed that nitrogen is also being incorporated in to allow for charge compensation.

3.5 Outlook and Future Work

There are still obstacles to overcome to improve these syntheses and further understand how nitrogen is incorporating into these structures. The main current issue is the difficulty in getting rid of the excess salt flux, KCl that is left after reaction. The reactions included in this work were all washed in air with methanol, but non-insignificant amounts of KCl were seen in the PXRD patterns. An attempt at washing the powder with THF was done, but this proved to be an even less effective solvent than methanol. In the future, use of DMF or DMSO as a washing solvent can be tested and might lead to better results.

It is also important to do experiments to determine the true composition and incorporation of nitrogen into the final product. PXRD is unable to differentiate between oxygen and nitrogen atoms as they differ in contrast by only one electron. Initial investigations other than PXRD could include energy-dispersive X-ray spectroscopy (EDS) and thermogravimetric analysis (TGA). EDS can be used to asses composition and homogeneity. [13] TGA can be performed in air and be used to identify the exchange of nitride for oxide. The weight of the sample would change if nitrogen is present in the structure which would be exchanged for oxygen during the analysis. [27] The Kjeldahl method can also be used as an analytical method to detect nitrogen in bulk samples. With this method, nitrogen is converted to dissolved NH_3, which can then be titrated with acid. [39] Lastly, the combination of advanced structural characterization methods can be used to locate nitrogen and oxygen in the crystal structure. Neutron diffraction can be performed at user facilities as a means for oxynitride formation confirmation. Unlike with X-rays, oxygen and nitrogen can be differentiated with neutrons owing to the difference in their neutron scattering lengths (b_c = 5.803 fm for oxygen and b_c = 9.36 fm for nitrogen). This difference provides significant enough contrast to allow for quantitative refinement of the chemical occupanices with the Rietveld method. [6] High-resolution synchrotron X-ray powder diffraction can also be used to determine metal-anion bond lengths which will allow for discrimination between oxygen and nitrogen in a bond-valence sum analysis.

Bibliography

[1] Y Taguchi, T Kawabata, T Takano, A Kitora, K Kato, M Takata, and Y Iwasa. Isotope effect in Li_xZrNCl superconductors. *Physical Review B*, 76(6):064508, 2007.

[2] Hiroshi Kageyama, Katsuro Hayashi, Kazuhiko Maeda, J Paul Attfield, Zenji Hiroi, James M Rondinelli, and Kenneth R Poeppelmeier. Expanding frontiers in materials chemistry and physics with multiple anions. *Nature communications*, 9(1):1–15, 2018.

[3] Hiroshi Amano. Nobel lecture: Growth of GaN on sapphire via low-temperature deposited buffer layer and realization of p-type GaN by Mg doping followed by low-energy electron beam irradiation. *Reviews of Modern Physics*, 87(4):1133, 2015.

[4] Yawei Wang, Yuyang Kang, Huaze Zhu, Gang Liu, John TS Irvine, and Xiaoxiang Xu. Perovskite oxynitride solid solutions of $LaTaON_2$-$CaTaO_2N$ with greatly enhanced photogenerated charge separation for solar-driven overall water splitting. *Advanced Science*, 8(2):2003343, 2021.

[5] Wenhao Sun, Stephen T Dacek, Shyue Ping Ong, Geoffroy Hautier, Anubhav Jain, William D Richards, Anthony C Gamst, Kristin A Persson, and Gerbrand Ceder. The thermodynamic scale of inorganic crystalline metastability. *Science Advances*, 2(11):e1600225, 2016.

[6] Varley F Sears. Neutron scattering lengths and cross sections. *Neutron News*, 3(3):26–37, 1992.

[7] Nenian Charles, Richard J Saballos, and James M Rondinelli. Structural diversity from anion order in heteroanionic materials. *Chemistry of Materials*, 30(10):3528–3537, 2018.

[8] S Ya Istomin, J Köhler, and A Simon. Crystal structure of β-ZrNCl refined from x-ray powder diffraction data, electronic band structures of β-ZrNCl and superconducting Li_xZrNCl. *Physica C: Superconductivity*, 319(3-4):219–228, 1999.

[9] Mr Ohashi, S Yamanaka, M Sumihara, and M Hattori. Novel synthesis of the layer structured β-ZrNCl by the direct reactions of zirconium metal or zirconium hydride with ammonium chloride. *Journal of Solid State Chemistry*, 75(1):99–104, 1988.

[10] Paul K Todd, M Jewels Fallon, James R Neilson, and Andriy Zakutayev. Two-step solid-state synthesis of ternary nitride materials. *ACS Materials Letters*, 3(12):1677–1683, 2021.

[11] B Song, JK Jian, G Wang, M Lei, YP Xu, and XL Chen. Facile and general route to nitrides by a modified solid-state metathesis pathway. *Chemistry of materials*, 19(6):1497–1502, 2007.

[12] Allison Wustrow and James R Neilson. Metathesis routes to materials. 2022.

[13] Christopher L Rom, M Jewels Fallon, Allison Wustrow, Amy L Prieto, and James R Neilson. Bulk synthesis, structure, and electronic properties of magnesium zirconium nitride solid solutions. *Chemistry of Materials*, 33(13):5345—-5354, 2021.

[14] Xiaohui Liu, Claudia Wessel, Fangfang Pan, and Richard Dronskowski. Synthesis and single-crystal structure determination of the zinc nitride halides Zn_2NX (x= Cl, Br, I). *Journal of Solid State Chemistry*, 203:31–36, 2013.

[15] Yanqing Li, Xiaohui Liu, and Richard Dronskowski. Synthesis and structure determination of the quaternary zinc nitride halides $Zn_2NX_{1-y}X_y$ (x, x= cl, br, i; 0< y< 1). *Inorganics*, 4(4):29, 2016.

[16] Yanqing Li, Janine George, Xiaohui Liu, and Richard Dronskowski. Synthesis, structure determination and electronic structure of magnesium nitride chloride, Mg_2NCl. *Zeitschrift für Anorganische Und Allgemeine Chemie*, 641(2):266–269, 2015.

[17] Rupert Marx. Preparation and crystal structure of lithium nitride chloride Li_4NCl. *Journal of Solid State Chemistry*, 128(2):241–246, 1997.

[18] JC Fitzmaurice, A Hector, and IP Parkin. Rapid synthesis of TiN, HfN and ZrN from solid-state precursors. *Polyhedron*, 12(11):1295–1300, 1993.

[19] Mayumi B Takeyama, Atsushi Noya, and Kouichirou Sakanishi. Diffusion barrier properties of ZrN films in the Cu/Si contact systems. *Journal of Vacuum Science & Technology B: Microelectronics and Nanometer Structures Processing, Measurement, and Phenomena*, 18(3):1333–1337, 2000.

[20] William D Richards, Lincoln J Miara, Yan Wang, Jae Chul Kim, and Gerbrand Ceder. Interface stability in solid-state batteries. *Chemistry of Materials*, 28(1):266–273, 2016.

[21] Takayuki Chiba, Keigo Hoshi, Yong-Jin Pu, Yuya Takeda, Yukihiro Hayashi, Satoru Ohisa, So Kawata, and Junji Kido. High-efficiency perovskite quantum-dot light-emitting devices by effective washing process and interfacial energy level alignment. *ACS Applied Materials & Interfaces*, 9(21):18054–18060, 2017.

[22] Andrew M Fogg, Victoria M Green, and Dermot O'Hare. Superconducting metallocene intercalation compounds of β-ZrNCl. *Chemistry of Materials*, 11(2):216–217, 1999.

[23] TF Ciszek, TH Wang, MR Page, RE Bauer, and MD Landry. Solar-grade silicon from metallurgical-grade silicon via iodine chemical vapor transport purification. In *Conference Record of the Twenty-Ninth IEEE Photovoltaic Specialists Conference, 2002.*, pages 206–209. IEEE, 2002.

[24] Liu Hongtao, Sang Wenbin, Min Jiahua, and Zhan Feng. Purification of $Cd_{0.9}Zn_{0.1}Te$ by physical vapor transport method. *Materials Letters*, 59(29-30):3837–3840, 2005.

[25] Y Taguchi, A Kitora, and Y Iwasa. Increase in Tc upon reduction of doping in Li_xZrNCl superconductors. *Physical Review Letters*, 97(10):107001, 2006.

[26] Amparo Fuertes. Synthetic approaches in oxynitride chemistry. *Progress in Solid State Chemistry*, 51:63–70, 2018.

[27] Stefan G Ebbinghaus, Hans-Peter Abicht, Richard Dronskowski, Thomas Müller, Armin Reller, and Anke Weidenkaff. Perovskite-related oxynitrides–recent developments in synthesis, characterisation and investigations of physical properties. *Progress in Solid State Chemistry*, 37(2-3):173–205, 2009.

[28] Ann L Greenaway, Celeste L Melamed, M Brooks Tellekamp, Rachel Woods-Robinson, Eric S Toberer, James R Neilson, and Adele C Tamboli. Ternary nitride materials: Fundamentals and emerging device applications. *Annual Review of Materials Research*, 51:591–618, 2021.

[29] H Yokokawa. Generalized chemical potential diagram and its applications to chemical reactions at interfaces between dissimilar materials. *Journal of Phase Equilibria*, 20(3):258–287, 1999.

[30] Erik G Rognerud, Christopher L Rom, Paul K Todd, Nicholas Ryan Singstock, Christopher J Bartel, Aaron M Holder, and James R Neilson. Kinetically controlled low-temperature solid-state metathesis of manganese nitride Mn_3N_2. *Chemistry of Materials*, 31(18):7248–7254, 2019.

[31] Hermann Schmalzried. *Chemical Kinetics of Solids*. John Wiley & Sons, 2008.

[32] Paul K Todd, Matthew J McDermott, Christopher L Rom, Adam A Corrao, Jonathan J Denney, Shyam S Dwaraknath, Peter G Khalifah, Kristin A Persson, and James R Neilson. Selectivity in yttrium manganese oxide synthesis via local chemical potentials in hyperdimensional phase space. *Journal of the American Chemical Society*, 143(37):15185–15194, 2021.

[33] SA Slater, WE Miller, and JL Willit. Precipitation of metal nitrides from chloride melts. Technical report, Argonne National Lab., 1996.

[34] Toru H Okabe, Akiyoshi Horiuchi, Kallaracke T Jacob, and Yoshio Waseda. Electrochemical properties of Li_3N dissolved in molten LiCl at 900 K. *Journal of The Electrochemical Society*, 148(5):E219, 2001.

[35] Toru H Okabe, Akiyoshi Horiuchi, Kallarackel T Jacob, and Yoshio Waseda. Physicochemical studies of lithium nitride in molten LiCl-KCl. *Materials Transactions, JIM*, 41(7):822–830, 2000.

[36] Robert J Sullivan, Thallam T Srinivasan, and Robert E Newnham. Synthesis of V_2O_3 powder by evaporative decomposition of solutions and H_2 reduction. *Journal of the American Ceramic Society*, 73(12):3715–3717, 1990.

[37] Serena A Corr, Daniel P Shoemaker, Brent C Melot, and Ram Seshadri. Real-space investigation of structural changes at the metal-insulator transition in VO_2. *Physical Review Letters*, 105(5):056404, 2010.

[38] B Zachau-Christiansen, K West, and T Jacobsen. Lithium insertion into VO_2 (b). *Materials Research Bulletin*, 20(5):485–492, 1985.

[39] LD Keele. Determination of nitrogen in boron nitride. Technical report, Union Carbide Corp., Oak Ridge, Tenn. Y-12 Plant, 1970.